NAR Molecular Medicine, 2026, **3**, ugag004
https://doi.org/10.1093/narmme/ugag004
Advance access publication date: 14 January 2026
Repeat Expansion Diseases

FMR1 RNA interaction with DNMT1 blocks DNA methylation at the *FMR1 locus*

Veronica Nobile[1,2,†], Benedetta Niccolini[1,2,3,†], Cecilia Pucci[1], Roberta Pietrobono[1,2], Clarissa Modafferi[3], Carla Lucia Esposito[4], Natalia Cappoli[2,5], Giada Bianchetti[6], Giuseppe Maulucci[2,6], Giuseppe Aceto[2,7], Marcello D'Ascenzo[2,7], Pietro Chiurazzi[1,2,3], Cinzia Dello Russo[2,5,8], Maurizio Genuardi[1,2,3], Giovanni Neri[1], Annalisa Di Ruscio[9,10,11,12], Elisabetta Tabolacci[1,2,3,*]

[1]Dipartimento di Scienze della Vita e Sanità Pubblica, Sezione di Medicina Genomica, Università Cattolica del Sacro Cuore, Largo F. Vito 1, 00168 Rome, Italy
[2]Fondazione Policlinico Universitario A. Gemelli IRCCS, 00168 Rome, Italy
[3]UOC Genetica Medica, Fondazione Policlinico Universitario A. Gemelli IRCSS, 00168 Rome, Italy
[4]Istituto degli Endotipi in Oncologia, Metabolismo e Immunologia "G. Salvatore" (IEOMI)-CNR, 80100 Naples, Italy
[5]Dipartimento di Sicurezza e Bioetica, Sezione di Farmacologia, Università Cattolica Del Sacro Cuore, 00168 Rome, Italy
[6]Dipartimento di Neuroscienze, Metabolic Intelligence Lab, Università Cattolica del Sacro Cuore, Largo Francesco Vito, 1, 00168 Rome, Italy
[7]Dipartimento di Neuroscienze, Università Cattolica del Sacro Cuore, 00168 Rome, Italy
[8]Department of Pharmacology & Therapeutics, Institute of Systems Molecular and Integrative Biology (ISMIB), University of Liverpool, L69 3GL Liverpool, United Kingdom
[9]Harvard Medical School Initiative for RNA Medicine, Harvard Medical School, Boston, MA 02115, United States
[10]Harvard Stem Cell Institute, Harvard Medical School, Boston, MA 02115, United States
[11]Cancer Research Institute, Beth Israel Deaconess Medical Center, Boston, 330 Brookline Avenue Boston, MA 02215, United States
[12]Beth Israel Deaconess Medical Center, Department of Medicine, Division of Hematology-Oncology, Boston, MA 02115, United States

*To whom correspondence should be addressed. Email: elisabetta.tabolacci@unicatt.it
†The two authors equally contributed to the work.

Abstract

In the *FMR1* gene, expansion of the CGG triplet beyond 200 repeats triggers DNA methylation, resulting in the Fragile X Syndrome (FXS). There exist rare individuals who carry a CGG expansion >200 that remains unmethylated, rescuing them from expressing the FXS phenotype. We tested the hypothesis that active *FMR1* transcription regulates DNA methylation of the locus through the binding of its mRNA to DNMT1 enzyme. Our results show that DNMT1 binds *FMR1*–mRNA in transcriptionally active cells preventing them from being methylated, whereas it binds to the *FMR1* locus in FXS cells, resulting in gene silencing. DNMT1 binds to the transcript or to the locus after reactivating or blocking *FMR1* transcription using specific drugs, respectively. As proof of concept, aptamers capable of binding and inhibiting DNMT1 were shown to reactivate the silenced *FMR1* gene. We propose that DNMT1 represents a specific molecular target to reactivate the *FMR1* gene expression.

Graphical abstract

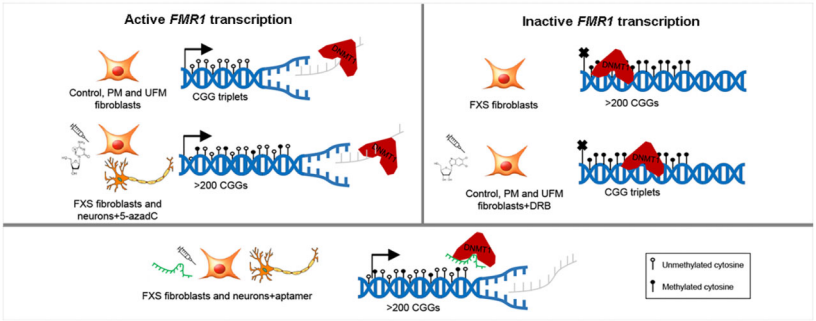

Received: September 9, 2025. **Revised:** December 17, 2025. **Accepted:** January 2, 2026

Introduction

FMR1 is the causative gene of Fragile X syndrome (FXS; OMIM #300624). Based on the number of CGG repeats, two major pathogenic alleles can be distinguished: alleles with 56–200 repeats are defined as premutation alleles (PM), whereas alleles with >200 repeats, followed by cytosine methylation, define the transcriptionally inactive full mutation allele (MFM) associated with the FXS phenotype. Exceptionally, CGG repeats exceeding 200 units may remain unmethylated, defining the rare unmethylated full mutation (UFM) allele [1, 2].

Although the precise mechanisms regulating the *FMR1* locus remain unclear, several epigenetic events are known to contribute to its silencing. Cytosine methylation, histone modifications, and chromatin remodeling represent the best-characterized factors involved in gene repression [3]. MFM alleles maintain a transcriptionally non-permissive heterochromatic configuration, whereas wild-type (WT) alleles are characterized by an "open" euchromatic structure that allows transcription. In general, the switch from active transcription to transcriptional silencing is a direct consequence of CGG repeat expansion beyond 200 units and the associated epigenetic modifications [3]. However, the existence of UFM alleles, in which *FMR1* transcription persists despite CGG expansions exceeding 200 repeats, indicates that additional mechanisms are involved in the maintenance of gene expression and silencing. Transcriptional regulation is critical for the activity of many genes. While MFM alleles are transcriptionally inactive, resulting in a loss-of-function effect, PM and UFM alleles are transcriptionally overactive, leading to a toxic gain-of-function effect of the RNA transcript [4, 5].

The formation of secondary structures in nascent RNA or DNA strands during transcription plays a critical role in the epigenetic regulation of many genes. One such structure is the R-loop, whose formation depends on multiple factors. Transcription through the GC-rich 5′ untranslated region (5′UTR) of *FMR1* favours R-loop formation [6]. The non-template strand of *FMR1* contains regions that are refractory to bisulfite footprinting, suggesting the presence of hairpin-like structures, consistent with the well-documented propensity of CGG trinucleotide repeats to form higher-order structures [6]. During transcription, the nascent RNA strand can invade the double-stranded DNA and anneal to the antisense template strand, forming a Watson–Crick DNA:RNA hybrid and displacing the non-hybridized strand as single-stranded DNA (ssDNA) [7]. R-loops are closely associated with antisense transcription and can promote antisense gene expression [8]. Moreover, R-loops at CpG islands (CGIs) within promoter regions play an important physiological role by protecting CpG-rich sequences from DNA methylation and epigenetic silencing. The combination of GC skew, G-rich sequences, free RNA, and the presence of DNA secondary structures creates an optimal genomic environment for R-loop formation [9, 10].

Multiple lines of evidence suggest that transcriptional activity is required to protect CGI promoters from DNA methylation. R-loop formation can shield these regions from DNMT3B1-mediated DNA methylation during early developmental stages [9]. More recently, R-loop formation has been shown to promote transcription by preventing methylation-induced silencing. Specifically, a reduction in R-loops exposes the *BAMBI* promoter and facilitates its methylation by DNA methyltransferase 1 (DNMT1). BAMBI is a negative regulator of transforming growth factor β (TGF-β); consequently, its silencing leads to activation of TGF-β signaling [11].

Although, in the context of FXS, R-loops are mostly considered promoters of *FMR1* transcriptional activity [6, 9, 12, 13], Colak *et al.* [14] suggested that disrupting the interaction between *FMR1* mRNA and the complementary CGG-repeat region of the gene using a small molecule known as 1a prevents promoter silencing.

R-loops are dynamic structures whose homeostasis must be finely regulated. Their dysregulation is implicated in several human diseases, including cancer and neurodegenerative disorders, underscoring their critical role in physiological processes. R-loops are involved in numerous cellular functions, such as regulation of gene expression, DNA repair, maintenance of chromosome structure and accessibility, induction of cell cycle checkpoints, chromosome rearrangements, DNA and histone modifications, immunoglobulin class-switch recombination, DNA replication, genome stability, telomere maintenance, and centromeric function [15, 16]. Furthermore, R-loops are closely associated with epigenetic mechanisms regulating transcription, including DNA methylation and post-translational histone modifications [9, 17], as well as with efficient transcriptional elongation, termination, polyadenylation, RNA splicing, packaging, and nuclear export [13].

The involvement of R-loops in repeat-expansion diseases is not limited to trinucleotide repeats. Indeed, R-loops associated with expanded G4C2 hexanucleotide repeats in the *C9ORF72* gene contribute to the molecular events underlying amyotrophic lateral sclerosis (ALS) and frontotemporal dementia [18]. Moreover, mutations in the putative RNA/DNA helicase *SETX* (senataxin) cause neurodegenerative disorders, including the dominant juvenile form of amyotrophic lateral sclerosis type 4 (ALS4) and the recessive ataxia oculomotor apraxia type 2 (AOA2) [19], highlighting the importance of proper regulation of R-loop levels in human cells [13].

Recent evidence indicates that R-loops can directly influence multiple gene expression–associated processes, including DNA methylation and transcription [13]. Using the *CEBPA* gene as a model, Di Ruscio *et al.* [20] demonstrated the existence of RNAs that interact with DNMT1. These DNMT1-interacting RNAs act as epigenetic modulators by inhibiting DNMT1 enzymatic activity, thereby preventing DNA methylation and transcriptional silencing of the associated genes. A direct role for DNMT1 at the *FMR1* locus has never been conclusively demonstrated; however, a recent study reported *FMR1* reactivation following DNMT1 targeting via CRISPR–Cas9 genome editing [21]. In addition, reactivation experiments using demethylating agents such as 5-aza-2′-deoxycytidine (5-azadC) or 5-azacytidine (5-azaC) have indirectly supported a role for DNMT1 in *FMR1* gene silencing [22–24].

An open question remains as to how such regulatory mechanisms are established. One possibility is that R-loops involved in gene regulation are spatially separated from the transcription start sites (TSSs) of the genes they control. Alternatively, when located within promoters or gene bodies, the processing of regulatory R-loops—namely their recognition, interpretation, and eventual removal—may be temporally uncoupled from transcription, for example occurring at specific stages of the cell cycle [16].

Here, we report on the role of the interaction between *FMR1* and DNMT1 in regulating the activity of the *FMR1* locus through a DNA methylation/demethylation mechanism. In addition, we explored an innovative RNA-based approach using aptamers to modulate DNMT1 activity in FXS, proposing an alternative strategy to overcome the limitations of currently approved non-specific hypomethylating therapies [25]. Aptamers are single-stranded synthetic oligonucleotides (RNA or DNA) that fold into defined three-dimensional structures and bind specific targets, such as proteins [26]. By combining the intrinsic ability of RNA to inhibit DNMT1 with the target specificity of aptamers, we aim to selectively regulate DNMT1 activity, thereby preventing methylation of the *FMR1* locus, which is considered the primary molecular cause of FXS.

Materials and methods

Cell lines and treatments

Fibroblasts derived from three different unaffected control males (CTRL), three different affected FXS patients, two UFM, and three PM carriers were employed. Their origin and characterization at the *FMR1* locus are reported in Supplementary Table S1.

Fibroblasts were established from skin biopsies obtained after a signed informed consent of each participant and anonymously established at the Section of Genomic Medicine at the Catholic University (Rome; Ethics Committee at the Catholic University of Rome approval N. 15152/15). Cell cultures were grown in DMEM (Sigma–Aldrich), supplemented with 10% fetal bovine serum (FBS), 1% penicillin/streptomycin, and 2.5% L-glutamine at 37°C with 5% CO_2.

Induced Pluripotent Stem Cells (iPSCs) and their derived neurons were the same described in Brykczynska *et al.* [27]. They were derived from two unrelated controls, two UFM derived from two unrelated individuals (see Supplementary Table S1), and two FXS patients. Protocols used for maintaining and differentiation were already published [27].

The DRB, 5,6-diclorobenzimidazolo 1-β-D-ribofuranoside (Sigma), was diluted in Dimethyl sulfoxide (DMSO). Time and concentration curves set the future treatments at 150 μM of concentration for 48 and 72 h. The compound was added once and after 48 or 72 h cells were harvested for subsequent experiments. Cells were also treated with DMSO, the diluent of used to dissolve DRB, representing negative control.

5-azadC (Sigma) was diluted in physiological solution and then added daily to the cells at a concentration of 5 μM for 1 week. One week after the beginning of the treatment, reactivation of the *FMR1* locus was first verified by quantitative PCR (qPCR) and then cells were harvested for the following studies.

qPCR

Total RNA was extracted using Trizol (Invitrogen). For a quantitative estimate of the *FMR1* and *DNMT1* mRNA levels, we performed a relative quantification with TaqMan probes, using an ABI7900HT (Thermo fisher). The TaqMan probes were the following: *FMR1* (IDT, Hs.PT.58.310966), *DNMT1* (IDT, Hs.PT.58.28037916), and *GAPDH* (IDT, Hs.PT.39a.22214836). The relative amount of target mRNA was assessed by comparison with the human *GAPDH* mRNA and using the Δc_t method.

Western blotting analysis

Proteins extracted from cells were resuspended in Laemli buffer, denatured, separated on 8% polyacrylamide gel electrophoresis, transferred to Immobilon-P membrane (Millipore), immunostained, and visualized using the ECL Western Blotting Kit (GE Healthcare), according to the manufacturer. Primary antibodies were used at the following concentrations: 1:500 anti-FMRP rabbit polyclonal antibody (Abcam, ab17722), 1:500 anti-DNMT1 mouse monoclonal antibody (Abcam, ab13537), and 1:25 000 anti-GAPDH rabbit polyclonal antibody (Abcam, ab9485). Protein quantification was obtained by densitometric measurements of the signal intensity after film exposure (ECL).

siRNA against DNMT1 transcripts

Primary fibroblasts were seeded at 1×10^5 cells in six-well dishes. Cells were transfected with 25 nM siRNA against *DNMT1* transcript (Silencer® Select Pre-designed siRNA, Thermofisher) and non-targeting control siRNA (scramble siRNA, IDT) using Lipofectamine RNAiMax (Invitrogen). Three different siRNAs were selected to ensure proper silencing of the *DNMT1*-mRNA (Cat. Num.4390824: ID s4215, s4216, s4217) and directed against exons 6, 25, and 26. The siRNAs were used in combination. Cells were harvested for expression analysis 24, 48, 72 h, 5 days, and one week from transfection (Supplementary Fig. S1C showed results after 72 h; other time points not shown) then collected for qPCR, WB, and ChIP assay. Scramble RNA and Lipofectamine alone (vehicle) were used as negative controls. Three independent transfections were performed.

Aptamer transfection

Anti-DNMT1 aptamer (ce-49 sh: 5′-CUGAGGCCUAACGAAGGCUUCU-3′) was transfected to FXS fibroblasts and iPSC-derived neurons using Lipofectamine 2000 (Invitrogen), according to the manufacturer's protocol. Aptamer was produced by the DNA/RNA Synthesis Laboratory, Beckman Research Institute of City of the Hope with 2′-F-Py all along the sequence. Cells were transfected with 100 nM of RNAs previously subjected to denaturation/renaturation steps as reported by Esposito *et al.* [25]. Cells were harvested for further analysis after 2 and 3 aptamer additions. The second and third addition were administered 72 h after the previous.

RNA immunoprecipitation

Nuclear and cytoplasmatic proteins were extracted from fibroblasts using NE-PER kit (Thermo Fisher) plus RNase inhibitor. Around 700–1000 μg of each extract was precipitated by 10 μg of antibody against DNMT1 (Abcam) through magnetic beads, Dynabeads Protein G (Life technologies). Negative control was immunoprecipitation with antibody against IgG rabbit (Abcam). An aliquot of each protein extract prior to immunoprecipitation was kept aside as input control. First, the immunoprecipitation protein enrichment was checked by western blot using 1:500 rabbit monoclonal antibody against DNMT1 (Abcam), 1:25 000 rabbit monoclonal antibody against GAPDH (Abcam). Thus, immunoprecipitated RNA was extracted following Trizol protocol (Life technologies), and the corresponding complementary DNA (cDNA) was quantified relative to the input RNA/cDNA (before IP)

through qPCR (ABI7900HT, Life Technologies). Three independent experiments were performed.

Chromatin immunoprecipitation assay and IP-DNA quantification

To study the binding between DNMT1 and *FMR1* locus, chromatin immunoprecipitation (ChIP) assay was performed on cells, according to the manufacturer (Millipore). The analysis was performed using the antibody against DNMT1. In each ChIP assay input DNA (prior immunoprecipitation) and no antibody sample (without antibody addition) were included as controls in each assay. Immunoprecipitated DNA (IP-DNA) was extracted by standard procedure (phenol/chloroform/isoamyl alcohol 25:24:1) and then quantified by absolute qPCR (ABI7900HT, Life Technologies) using fluorescent probes and primers specific for both *FMR1* (promoter region, exons 1 and 16) and *HPRT*, as already published [2]. Probes for exon 16 of the *FMR1* gene and *HPRT* were used as negative controls.

Standard curves for both *FMR1* and *HPRT* amplicons were constructed with five DNA dilutions at known concentration [X axis = log(X)] and the corresponding Ct values (Y-axis). The unknown amount of IP-DNA of *FMR1* and *HPRT* [X-axis = log(X)] was calculated from Ct values, through the standard curve plot [$y = ax + b$, that is $Ct = ax + b$, with x = log(X)]. The values of IP-DNA were expressed in the graphs as a percentage (%) of ng of IP-DNA versus ng of input DNA or ng of no Ab DNA versus ng of input DNA. Three independent experiments were performed.

DNA:RNA hybrid immunoprecipitation (DRIP)

Cells were manually detached and lysed adding protease inhibitors. DNA was fragmented by sonication and a small amount was kept aside as input control, while the rest was pretreated, or not, with RNaseH. For DNA:RNA immunoprecipitation (DRIP), DNA was immunoprecipitated with S9.6 antibody (Merck). After an overnight immunoprecipitation with S9.6 antibody, the IP-DNA (including input and RNaseH digested samples) was purified through Wizard® DNA Clean-Up system (Promega, cat. A7280). DNA samples were quantified by absolute qPCR (ABI7900HT, Life Technologies) using fluorescent probes and primers specific to the *FMR1* gene (promoter region, exons 1 and 16), promoter of *GAPDH* and *MYADM* gene. Three independent experiments were performed.

RNase H hydrolyzes the RNA in R-loops structures [28, 29] and it is used in several studies to validate the specificity of the S9.6 antibody binding. We showed that our S9.6 signal is abolished by treatment with RNase H, as expected.

Exon 16 of *FMR1* gene and promoter of *GAPDH* gene represented negative controls for the presence of hybrids, while *MYADM* gene represented positive control [6]. FXS cell lines were included as negative control for absence of *FMR1* transcription. The values of IP-DNA were expressed in the graphs as a percentage (%) of ng of IP-DNA versus ng of input DNA or ng of RNaseH DNA versus ng of input DNA.

DNMT1 assay

A commercial DNMT activity/inhibition assay (Active Motif, #55006) was used to quantify DNMT1 binding and activity. In this assay, we pre-incubated double strand DNA (dsDNA) or DNA:RNA hybrid containing the 5′UTR of the *FMR1* gene with recombinant DNMT1. We designed three oligomers as competitors to the CpG substrate: the dsDNA mapping to exon1 of *FMR1* gene (dsDNA) and two DNA:RNA hybrids, one with the template DNA and the complementary RNA (hybrid 1) and the other with the non-template strand DNA and its complementary RNA (hybrid 2). The sequences of oligonucleotides (IDT) were reported in Supplementary Table S2. After pre-incubation phase, it was measured the methylation of CpG-rich sequences that were immobilized on 96-well plates. DNMT1 transfers the methyl group from S-adenosyl methionine (SAM) supplied in the reaction kit to the immobilized DNA, and the methylated cytosine was quantified by ELISA assay with a specific methyl-binding protein and HRP-conjugated antibody. 500 ng of recombinant DNMT1 (Active Motif) was incubated with a titration of dsDNA or DNA:RNA hybrid at 25°C for 30 min in 10 µl binding buffer (10 mM Tris–HCl, pH 7.5, 150 mM NaCl). Methylation level of CpG nucleotides by DNMT1 was measured by a microplate reader (Victor-X™4, PerkinElmer Inc.) set at 450 nm following manufacturer's manual. Each reaction was carried out in sextuplicate. DNMT1 activity on dsDNA or DNA:RNA hybrid was calculated as Activity = 1 − (OD_{450} of sample with competitor − OD_{450} background)/(OD_{450} sample without competitor – OD_{450} background). Average and SEM of replicates were reported. This assay measures the ability of DNMT1 to methylate CpG sites in the presence of binding to dsDNA or hybrids specific for *FMR1*.

Electrophoretic mobility shift assay

Electrophoretic mobility shift assay (EMSA) was carried out using biotinylated dsDNA or DNA:RNA hybrids with the sequence described in Supplementary Table S2. Serial titrations of recombinant DNMT1 were incubated with 0.1 nM of biotinylated nucleotide substrates in DNMT1 binding buffer [5 mM Tris–HCl, pH 7.4, 5 mM $MgCl_2$, 1 mM DTT, 3% (v/v) glycerol, and 100 mM NaCl] in a 10 ml reaction at room temperature for 30 min. For the competition assay, 100 nM of non-biotinylated dsDNA was added to the appropriate tubes and incubated for 15 min before the addiction of the biotinylated substrates. The 10 µl samples were mixed with 1.1 µl of Novex Hi-Density TBE Sample buffer (5×) and loaded to 6% DNA retardation gel (ThermoFisher, #EC6365BOX) and run at 100V in 0.5× TBE at 4°C for 1.5 h. The gel was blotted to Hybond N + nylon membrane in 0.5× TBE at 4°C at 15 V for 17 h. Biotin signal was detected using Chemiluminescent Nucleic Acid Detection Kit (ThermoFisher, #89880).

Biolayer interferometry

Analysis of dsDNA or DNA:RNA hybrid binding to DNMT1 was carried out using the Octet RED96 system (ForteBio) with sensor detection of the change in wavelength (nm shift). Biotinylated dsDNA or DNA:RNA hybrids specific to the 5′UTR of the *FMR1* gene (LRG_762) and double strand oligonucleotides mapping on exon 17 of *FMR1* gene, used as negative controls for dsDNA structures formation, were all purchased by IDT (Leuven, Belgium). The three oligomers for exon 17 of the *FMR1* gene have been designed adopting the same strategy of exon 1 [30]. The sequence of both series of double strand oligonucleotides are reported in Supplementary Table S2.

Both dsDNA and DNA:RNA hybrids were immobilized onto a Streptavidin-SA biosensor at 5 nM. Recombinant

DNMT1 (Active Motif, #55006) at concentrations of 8.89, 26.7, and 80 nM were loaded onto the sensors until saturation. The nucleotide-labeled sensors were then washed with buffer, followed by addition of DNMT1 at the three different concentrations. All reactions were tested in TBS buffer (10 mM Tris, pH 7.4, 68 mM NaCl, and 0.02% Tween-20). A reference sample of buffer and DNMT1 alone were used as negative controls. Association and dissociation were monitored for 10 min each with agitation at 1000 rpm.

Transformation with sodium bisulfite

Genomic DNA was isolated from DRB treated and untreated cells and from aptamer transfected and untransfected iPS-derived neurons by DNeasy Blood & Tissue kit (Qiagen, 69504). gDNA (genomic DNA) was transformed using EZ DNA Methylation kit (Zymo), and the transformed DNA was amplified, cloned, and sequenced including the 54 CpG of the *FMR1* promoter region, as already published [31, 32].

CGG sizing

CGG sizing of the aptamer transfected and 5-azadC-treated iPS-derived neurons was assessed by AmplideX® PCR assay (Asuragen, Austin, TX, USA), following manufacturer's protocol. Amplified products were visualized by capillary electrophoresis (3500xL Genetic Analyzer, Thermo Fisher, Waltham, MA, USA) and separated using POP-7™polymer (Thermo Fisher), following manufacturer's instructions. The size of the PCR products has been converted to the estimated number of CGG repeats using size and mobility conversion factors. The reference sequence of the *FMR1* gene used for sizing the CGG repeat is LRG_762 (identical to NG_007529.2).

Immunofluorescence and confocal analysis

For immunofluorescence analysis, we first fixed derived neurons with 3.7% formaldehyde for 15 min at RT, then permeabilized with 0.05% Triton X-100 in PBS and blocked with 5% bovine serum albumin (BSA) for 1 h at RT. Cells were incubated with the following primary antibodies: rabbit αMAP2 (against Microtubule-Associated Protein 2), rabbit αNeuN (against Neuronal Nuclei), and rabbit αGFAP (against Glial Fibrillary Acidic Protein) (Thermo Fisher). Then slices were incubated with goat Alexa Fluo-488 α-rabbit IgG and/or goat Alexa Fluo-594 α-rabbit IgG (Thermo fisher) and DAPI (4′,6-diamidino-2-phenylindole) counterstained. Cells were imaged with an inverted confocal microscope (Nikon A1-MP). Fluorescence images were collected on three separate channels (excitation: 402 nm, emission: 450/50 nm for the blue channel; excitation: 488 nm, emission: 525/50 nm for the green channel; excitation: 561 nm, emission: 595/50 nm for the red channel) using a ×60 oil-immersion objective with 1.4 numerical aperture (NA). Internal photon multiplier tubes collected images with pixel resolutions of 1024 × 1024 in 16 bit at 0.063 ms dwell time. Exposure and gain settings are kept constant across conditions.

Patch–clamp recordings on iPSCs derived neurons

Neuronal excitability was investigated using the whole-cell patch-clamp technique at room temperature (23–25°C), as previously described [33, 34]. Data acquisition was performed using a MultiClamp 700B amplifier (Molecular Devices) and digitized at 10 kHz with the Digidata 1440A data acquisition system (Molecular Devices). Data were analyzed using pClamp 11 software (Molecular Devices). The patch-clamp electrodes, with resistances ranging from 3 to 5 MΩ, were fabricated from borosilicate glass capillaries using a micropipette puller (PC-10; Narishige) and filled with an internal solution containing the following components (in mM): 130 K-gluconate, 10 KCl, 1 EGTA, 10 HEPES , 2 $MgCl_2$, 4 MgATP, and 0.3 Tris–GTP. Throughout the recordings, the cells were continuously perfused with Tyrode's solution, which consisted of (in mM): 140 NaCl, 2 KCl, 10 HEPES, 10 glucose, 1 $MgCI_2$, and 2 $CaCl_2$, with a pH of 7.4 and an osmolarity of 312 mOsm. All salts are purchased from Sigma–Aldrich. Evoked firing was recorded in current–clamp configuration following by a series of 400 ms current pulses (every 10 s) from −20 to 200 pA, 20 pA steps. For voltage-gated Na^+-currents, pipettes were filled with an intracellular solution comprised of the following salts: 120 CsCl, 10 NaCl; 20 TEA-Cl; 10 EGTA, 10 Hepes; 2 $MgCl_2$, 4 NaATP (pH 7.4 with CsOH). Neurons were perfused with an external Tyrode's solution containing the following (in mM): 135 NaCl, 1 $CaCl_2$; 2 $MgSO_4$, 10 HEPES, 10 glucose, 5 TEA-Cl; 4 $MgCl_2$, 4 $CaCl_2$, and 0.2 CdCl (pH 7.4; all salts purchased from Sigma–Aldrich). After GΩ seal formation and entry into the whole-cell configuration, the voltage–clamp protocols shown in Supplementary Fig. S7 were performed.

Statistical analysis

Unless stated otherwise in the figure legends, each experiment derives from at least three independent biological replicates. Data are expressed as mean ± SD. *P*-values indicated in the figures are calculated with GraphPad; Student's *t*-test and one-way ANOVA (only for data on Supplementary Fig. S7) are applied. The variance between the compared groups is similar. GraphPad (version 8.0.1) and ImageJ (version 1.53K) software were used to create the artwork.

Results

DNMT1 binds to both the FMR1 locus and its transcript

DNMT1 transcription and translation were quantified by qPCR and Western blot in FXS, UFM and PM fibroblasts compared to control. Although transcriptional levels of *DNMT1* appeared higher in UFM, PM, and FXS compared to controls (Supplementary Fig. S1A), its protein levels were equivalent in the different cell lines and to those of controls (Supplementary Fig. S1B). To examine the possible connection between *FMR1*–mRNA and DNMT1 levels, as a first point DNMT1 was knocked down with specific siRNA against *DNMT1* transcript in cells with inactive *FMR1* transcription, such as FXS fibroblasts. Despite efficient DNMT1 knockdown in FXS fibroblasts, no transcriptional reactivation of *FMR1* gene was observed after 24, 48, 72 h, 5 days, and one week (Supplementary Fig. S1C, 72 h; other time points not shown), and DNMT1 essentially remains bound to the *FMR1* locus (Supplementary Fig. S1D). Given these results, we hypothesized that the methylation status of the *FMR1* gene must depend on a more complex mechanism, probably involving other epigenetic modifiers/factors/pathways.

We then moved on to quantify R-loops at the *FMR1* locus in the four different types of fibroblasts. R-loops abundance at the *FMR1* locus was quantified using immunoprecipitation

with the well-established S9.6 antibody for the detection of DNA:RNA hybrids, in association with RNase H treatment to ensure specificity of the signals [35]. In the *FMR1* promoter region, UFM and PM cells showed a significant increase in R-loops compared to CTRL, while no R-loops were found in MFM (FXS) cells as expected (Fig. 1A). Similar results were obtained using specific primers for exon 1 of the *FMR1* gene (Supplementary Fig. S2A), while absence of hybrids was found at exon 16 of *FMR1* and at the promoter region of *GAPDH* (negative controls) (Supplementary Fig. S2B and C, respectively). *MYADM* represented a positive control for hybrids formation [6] (Supplementary Fig. S2D).

To investigate whether DNMT1 showed a different binding to *FMR1* locus in relation to the methylation status of the different alleles, ChIP assay with antibody against DNMT1 followed by IP-DNA absolute quantification with qPCR was performed in CTRL, PM, UFM, and FXS fibroblasts. FXS cells displayed a significant increase in DNMT1 amount bound to either the promoter region (Fig. 1B) or exon 1 of the *FMR1* gene (Supplementary Fig. S3A). Exon 16 of *FMR1* gene and *HPRT* were used as negative controls for DNMT1 binding (Supplementary Fig. S3B and C, respectively) [2]. Contrariwise, *FMR1* transcriptionally active cell lines do not show any binding of DNMT1 to the *FMR1* locus.

We then explored whether DNMT1 could bind the *FMR1* transcript in control, PM and UFM fibroblasts through RNA immunoprecipitation (RIP) using antibody against DNMT1 and quantifying *FMR1* transcript by qPCR. DNMT1 bound *FMR1*–mRNA transcript in transcriptionally active cells, i.e. control, PM, and UFM (Fig. 1C). In PM cell lines, DNMT1 bound the *FMR1* transcripts with affinity from 2 to 4 times higher than in CTRL. Instead, UFM cell lines showed about eight times more *FMR1*–mRNA bound to DNMT1 compared to control. FXS fibroblasts represent negative controls for the binding of DNMT1 to *FMR1* transcript.

In *FMR1* transcriptionally active cell lines DNMT1 did not bind to the *FMR1* locus but to the *FMR1* transcripts. Contrariwise, in *FMR1* transcriptionally inactive FXS fibroblasts, DNMT1 associates with the *FMR1* locus, whereas no binding to the *FMR1* transcript is detected, consistent with the absence of transcript in these cells.

How DNA methylation influences FMR1 transcription

Here, we aimed to investigate how nucleic acid structures related to the *FMR1* locus could influence DNMT1 activity. To address this point, we first examined whether DNA methyltransferase activity differs based on oligonucleotide substrates, in particular, dsDNA versus DNA:RNA hybrids designed for the *FMR1* locus. A competitive immunoassay was used to investigate the activity of recombinant DNMT1 on immobilized CpG-rich sequences, with dsDNA or corresponding DNA:RNA hybrids added as competitors. Binding of the methyl-C binding protein to immobilized substrates provides a colorimetric readout. Results from this assay are reported in Fig. 2A. The methylation activity is reduced when DNMT1 interacts with RNA/DNA1 (hybrid 1) formed by template DNA strand and its complementary RNA (specifically *FMR1* mRNA). In contrast, dsDNA was able to compete more effectively at lower concentrations, indicating it as the preferred substrate. Among the two hybrids, RNA/DNA1 inhibited DNMT1 more strongly than hybrid 2 (RNA/DNA2), designed between non-template DNA and antisense *FMR1* transcript.

EMSA was performed to test whether DNMT1 binding differs between dsDNA and DNA:RNA hybrids. Probes corresponding to the *FMR1* promoter region were used, both dsDNA and hybrid 1 based on the ELISA results. As showed in Fig. 2B, DNMT1 binds avidly to both dsDNA and RNA/DNA hybrid 1 already at lower DNMT1 concentrations. A reduced intensity of the DNMT1/oligos complex was observed with increasing concentrations of DNMT1, likely due to the formation of larger or heterogeneous complexes that migrate more slowly or remain trapped in the gel. Aggregation or oversaturation effects may also contribute to this observation.

Biolayer interferometry assays further confirmed that DNMT1 exhibits higher affinity for dsDNA than for the corresponding DNA:RNA hybrids designed on 5′UTR of the *FMR1* gene (Fig. 2C). Among the two hybrids, hybrid 1 binds more strongly to DNMT1 than hybrid 2. Oligonucleotides designed at exon 17 of the *FMR1* gene were used as negative control (Supplementary Fig. S4).

Taken together, these results indicate that, while DNMT1 can interact with specific DNA:RNA hybrids spanning the 5′UTR region of the *FMR1* gene, particularly those between template DNA and *FMR1* mRNA, its preferred substrate is dsDNA.

Transcriptional inhibition of the FMR1 locus recapitulates FXS condition

To better understand the correlation existing between the transcription and the DNA methylation status of the *FMR1* gene, we chose to pharmacologically inhibit the transcription, treating fibroblasts with 5,6-dichlorobenzimidazole 1-β-D-ribofuranoside (DRB). DRB is an inhibitor of RNA synthesis and causes premature termination of transcription. It is a nucleoside analog that halts mRNA synthesis by phosphorylation of the C-terminal domain of RNA polymerase II, making it inactive [36].

After treatment of all *FMR1* transcriptionally active fibroblasts (CTRL, PM, and UFM) a significant reduction in transcription and translation of the *FMR1* locus is observed, as expected (Supplementary Fig. S5A and B). To ascertain the reduction in transcription observed after DRB treatment corresponded to a proportional reduction in R-loops, we quantified R-loops through DRIP assay. As shown in Fig. 3A, R-loops in the *FMR1* promoter and exon 1 regions are reduced after treatment with DRB compared to the untreated controls (see Supplementary Fig. S5C for the other regions analyzed by DRIP as controls; data after RNase H digestion are not shown). We also showed that after DRB treatment the amount of DNMT1 bound to the *FMR1* promoter and exon 1 regions significantly increased in CTRL, UFM, and PM (Fig. 3B). The ChIP assay with antibodies against DNMT1 and the IP-DNA quantification with qPCR of exon 16 region of the *FMR1* gene and *HPRT* gene after DRB treatment are reported in Supplementary Fig. S5D.

To explore if these data correlate with DNA methylation levels at the *FMR1* locus, we analyzed the DNA methylation status at the *FMR1* promoter following bisulfite transformation of genomic DNA after DRB treatment. Interestingly, we observed that the reduction in transcription induced by the compound also stimulated a slight increase in DNA methylation at the *FMR1* promoter in CTRL cell line (Fig. 3C) and in

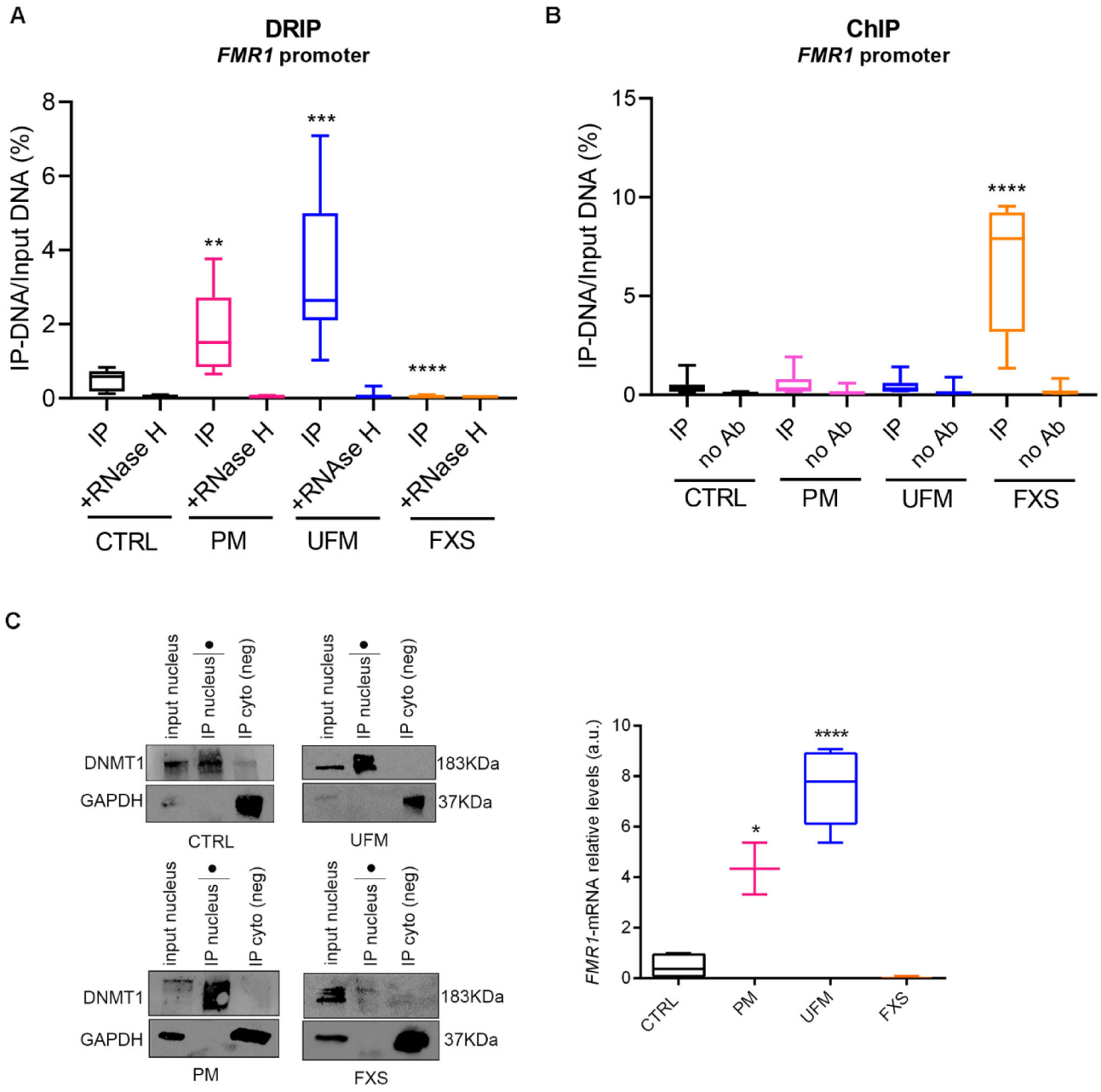

Figure 1. Quantification of R-loops and binding of DNMT1 to *FMR1* locus and transcript. (**A**) DNA:RNA hybrids immunoprecipitation (DRIP) using S9.6 antibody in PM, UFM, and FXS fibroblasts compared to control followed by absolute quantification of IP-DNA through qPCR using specific probe for *FMR1* promoter region. RNase H digested RNA in DNA:RNA hybrids ensuring the specificity of the signal. Four independent immunoprecipitations are performed ($n = 4$). The quantity of hybrids is significantly higher in PM and UFM and practically absent in FXS respect to control; $^{**}P < 0.01$, $^{***}P < 0.001$, $^{****}P < 0.0001$ (**B**) ChIP assay using antibody against DNMT1 in PM, UFM, and FXS fibroblasts compared to control followed by absolute quantification of IP-DNA through qPCR using specific probe for *FMR1* promoter region. All samples are treated as the corresponding immunoprecipitated but without adding the antibody (no Ab), thus representing negative control. Four independent immunoprecipitations are done ($n = 4$). Levels of DNA bound to DNMT1 at the *FMR1* promoter region are significantly higher in FXS cells compared to control, PM, and UFM; **** $P < 0.0001$. (**C**) RIP using antibody against DNMT1 (on the left) followed by relative quantification by qPCR of *FMR1* transcript bound to DNMT1 in PM, UFM, and FXS compared to control (on the right). Note the enrichment of DNMT1 in the nuclear fraction after IP, less visible in FXS fibroblasts (black dot). After IP *FMR1*–mRNA bound to DNMT1 is quantified using qPCR comparing each sample to the corresponding input RNA. Relative levels of *FMR1*–mRNA bound to DNMT1 were higher in PM and UFM compared to control and absent in FXS, as expected. Three independent RIPs are performed ($n = 3$); $^{*}P < 0.05$, $^{****}P < 0.0001$ (Student's *t*-test versus control).

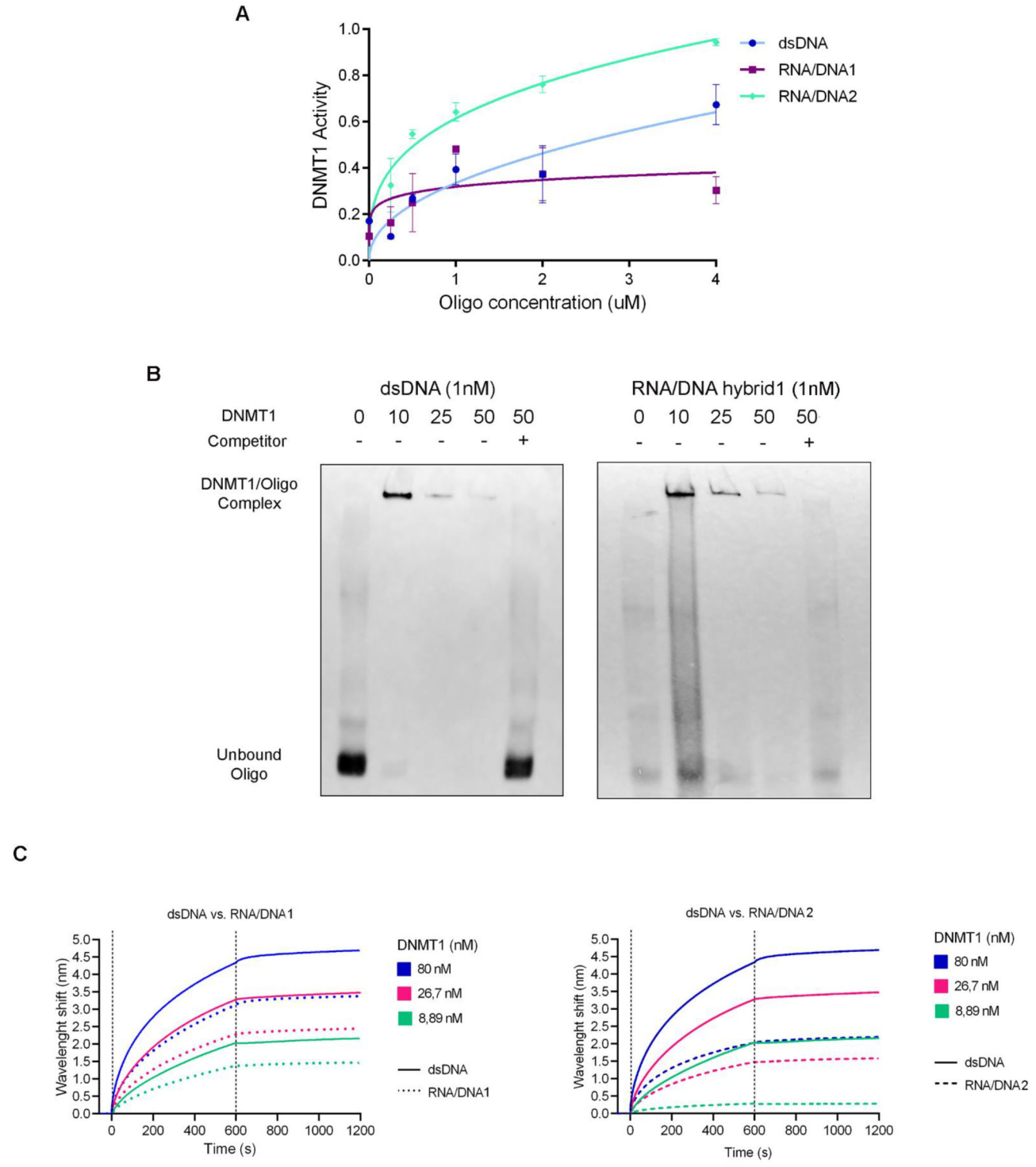

Figure 2. DNA methylation and *FMR1* transcription. (**A**) Competitive methylation ELISA assay using recombinant DNMT1 at different concentrations of *FMR1* 5′UTR oligonucleotides: dsDNA (blue), hybrid 1 (RNA/DNA1, formed by template DNA and *FMR1*–mRNA) (violet), and hybrid 2 (RNA/DNA2, designed between no template DNA and *FMR1* antisense transcript) (green). Adding serial concentrations of such oligonucleotides (up to 4 μM) as competitors to the recombinant DNMT1, hybrid 2 showed lower inhibition of DNMT1. Error bars represent SEM of triplicates. (**B**) EMSA using several concentrations (up to 50 nM) of recombinant DNMT1 and biotinylated [1 nM] oligonucleotides, one specific for the 5′UTR of *FMR1* (dsDNA) and the other for hybrid 1, without (−) or with (+) the preliminary addition of a dsDNA as a competitor. Note the binding of DNMT1 to both oligonucleotides, even at low concentrations of the recombinant enzyme. Adding the dsDNA as a competitor, the binding disappeared for both oligonucleotides. (**C**) Biolayer interferometry assay using recombinant DNMT1 at three serial concentrations (80, 26.7, and 8.89 nM) and specific 5′UTR of the *FMR1* dsDNA versus hybrid 1 (on the left) and dsDNA versus hybrid 2 (on the right). Note that hybrid 1 binds DNMT1 more avidly than hybrid 2.

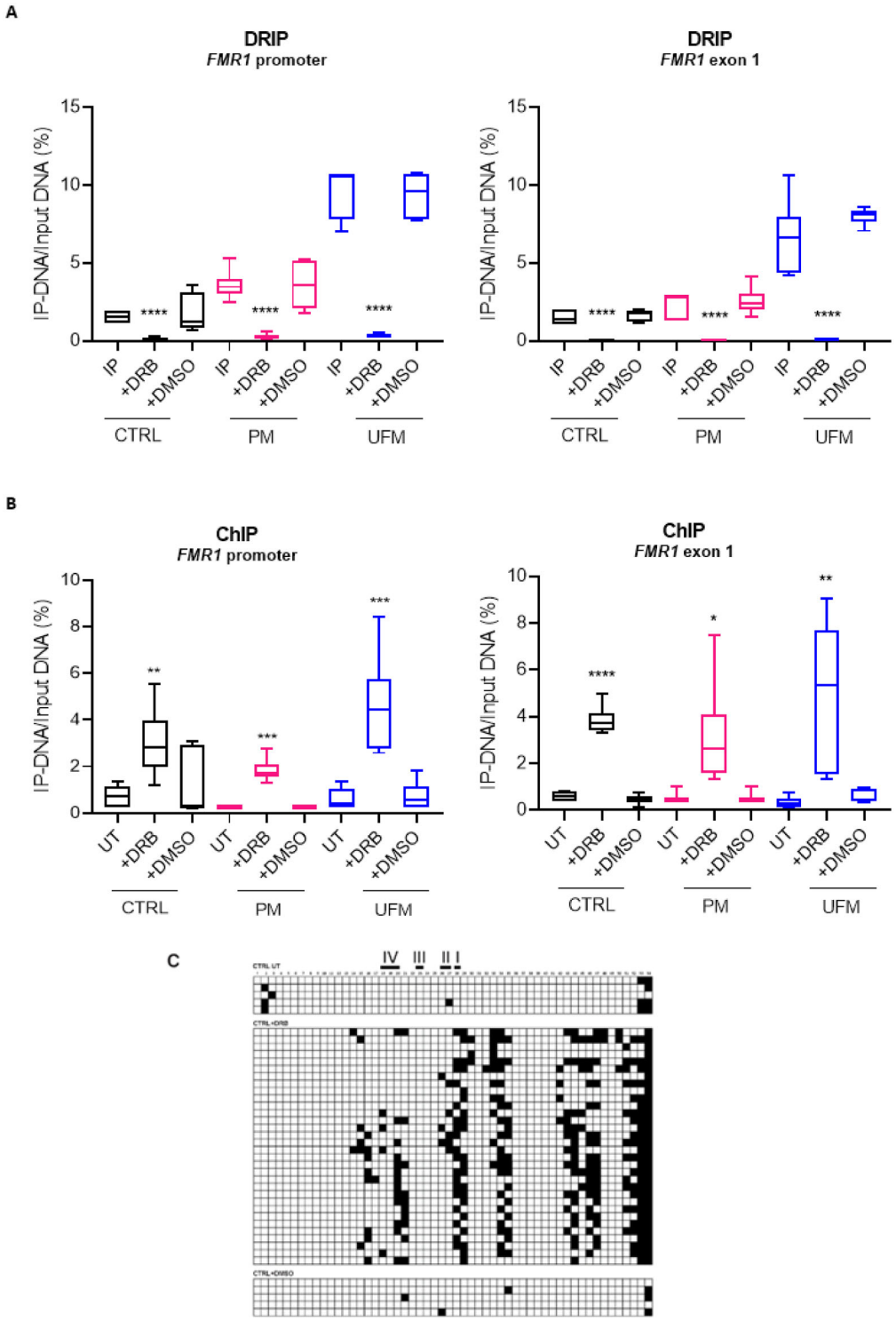

Figure 3. Transcriptional inhibition of the *FMR1* gene through DRB treatment of control, PM, and UFM fibroblasts. (**A**) DRIP assay in control, PM, and UFM fibroblasts followed by absolute quantification of IP-DNA through qPCR using specific probe for *FMR1* promoter (on the left) and exon 1 (on the right) regions. After transcriptional inhibition with DRB, levels of R-loops significantly decreased in control, PM, and UFM fibroblasts compared to the untreated cells. DMSO represented the diluent used to dissolve DRB and it is used as negative control. Three independent DRB treatments are done ($n = 3$); $****P < 0.0001$. (**B**) ChIP assay using antibody against DNMT1 in control, PM, and UFM fibroblasts treated with DRB compared to untreated controls followed by absolute quantification of IP-DNA through qPCR using specific probes for *FMR1* promoter (on the left) and exon 1 (on the right) regions. After transcriptional inhibition through DRB, levels of DNA bound to DNMT1 at the *FMR1* promoter and exon 1 regions are significantly higher in treated cells compared to untreated controls. DMSO represented the diluent used to dissolve DRB and it is used as negative control. Three independent immunoprecipitations are done ($n = 3$); $*P < 0.05$, $**P < 0.01$, $***P < 0.001$, $****P < 0.0001$ (Student's *t*-test versus untreated). (**C**) Bisulfite sequencing of the CGI of the *FMR1* promoter region after DRB treatment of control fibroblasts. White squares represented unmethylated cytosines, while black squares methylated positions. Binding sites for the main transcription factors are reported on the top (see also [31] and [32]). Note that after transcriptional reduction of *FMR1* transcription through DRB treatment of control cells, an increase in DNA methylation is observed. DMSO represented the diluent used to dissolve DRB and it is used as negative control.

both PM and UFM fibroblasts (Supplementary Fig. S5E and F).

When cell lines with active *FMR1* transcription are driven into inactive transcription status, the effect recapitulates the event leading to DNA methylation at the *FMR1* locus.

Transcriptional reactivation of the FMR1 gene restores "normal" conditions

Opposite to DRB treatment (inhibition of transcription) is the pharmacological re-activation of the *FMR1* locus in MFM cells using 5-azadC, a compound capable to demethylate this locus [22, 23, 31]. Two different FXS cell lines were daily treated with 5-azadC for one week and at the end of treatment we confirmed *FMR1* re-activation through qPCR and western blot (Supplementary Fig. S6A and B). In association with transcriptional reactivation, R-loops reappeared at the *FMR1* promoter and exon 1 regions, as shown in Fig. 4A. In Supplementary Fig. S6C, all amplified regions after DRIP as controls are reported. At this point the investigation of the DNMT1 behavior after pharmacological restoration of *FMR1* transcription was critical. Interestingly, we observed that, in treated FXS cells, the amount of DNMT1 bound to *FMR1* promoter and exon 1 regions significantly decreased compared to untreated cells (Fig. 4B). All ChIP data with antibodies against DNMT1 are reported in Supplementary Fig. S6D. Finally, following 5-azadC treatment and *FMR1* reactivation, a portion of the *FMR1* transcript appeared to be associated with DNMT1 as indicated by RIP results (Fig. 4C).

To extend these findings to neuronal target cells, FXS iPSCs derived neurons [27] were daily treated with 5-azadC for 7 days (Supplementary Fig. S7). After confirming *FMR1* reactivation (Figs 5A and 6C), we moved on to investigate the presence of DNA:RNA hybrids and the DNMT1 binding to the *FMR1* locus (Fig. 5B and C, respectively). The transcriptional reactivation of the *FMR1* gene lead to a reappearance of DNA:RNA hybrids (see Supplementary Fig. S8A for complete DRIP results) and to a decrease in the amount of DNMT1 bound to the 5′UTR of the gene (see Supplementary Fig. S8B for complete ChIP results), demonstrating that, when the *FMR1* transcription is pharmacologically re-activated, the corresponding DNA demethylation induces the reappearance of new R-loops also in target cells.

Taken together, these data showed that pharmacological demethylation induces the formation of hybrids and the removal of DNMT1 to the *FMR1* locus.

Effects of DNMT1 inhibition at the FMR1 locus using aptamer

A synthetic oligonucleotide (aptamer) able to selectively bind and inhibit DNMT1 [20, 25] was first used to transfect FXS fibroblasts (Supplementary Fig. S9), as proof of principle. Aptamer was added two or three times at two different FXS fibroblasts and it was shown to reactivate the silent *FMR1* gene, particularly after two additions. We then treated FXS derived neurons with two or three doses of aptamer to check for a reactivating effect on the *FMR1* gene. Surprisingly, aptamer caused a robust *FMR1* reactivation (Fig. 6A), similar to that observed in fibroblasts (Supplementary Fig. S9), including a partial DNA demethylation of the CGI at the *FMR1* promoter region (Fig. 6B) and restoration of FMRP production (Fig. 6C), especially after two administrations of the aptamer. Levels of reactivation after aptamer transfection appeared similar to those obtained with 5-azadC treatment. Furthermore, aptamer transfection did not apparently affect the size and integrity of the CGG expansion as observed through fluorescent PCR specific for CGG sizing (Supplementary Fig. S10). After reactivation of the *FMR1* gene using aptamer on FXS iPS-derived neurons, DNMT1 binding to the *FMR1* locus appeared significantly reduced in the 5' UTR region of the *FMR1* gene, i.e. promoter region and exon 1 (Fig. 6D and Supplementary Fig. S11).

Overall, these data highlighted the role of the aptamer as an agent capable of inhibiting DNMT1, thereby reactivating *FMR1* through its demethylation without affecting the integrity of the trinucleotide repeat. Reactivation of *FMR1* gene using aptamer able to inhibit DNMT1 in FXS–iPS-derived neurons paves the way for a possible approach to specifically demethylate genes in target cells.

Discussion

The DNMT1 enzyme is known for its crucial role in DNA methylation, usually active after S-phase of cell cycle and associated with hemimethylated DNA strand maintaining epigenetic modifications across cell divisions. Recent studies have highlighted the involvement of DNMT1 not only in methylating DNA but also in regulating gene expression through its interaction with specific genomic loci and transcript [37, 38]. In this study, we examine the interaction between DNMT1 and the *FMR1* gene, particularly focusing on its binding to both the gene's locus and its RNA product. This interaction has been shown to be closely linked to the transcriptional regulation of *FMR1* and is modulated by epigenetic modifications. This dual binding mechanism implicates DNMT1 in the regulation of gene transcription, providing further insight into the complexity of gene expression regulation beyond DNA methylation alone. The presence of DNMT1 at the *FMR1* locus appears to influence the expression of the gene, potentially through the establishment or maintenance of DNA methylation marks at critical regulatory regions. Though at low levels, DNMT1 binding to *FMR1* mRNA was already observed in leukemic cells [20]. RIP experiments clearly demonstrated the binding of *FMR1*–mRNA to DNMT1 in premutated and UFM cells. When *FMR1* transcript is absent, such as in FXS cells, DNMT1 binds only to *FMR1* locus maintaining its methylated and silenced status. The low DNMT1 enrichment observed in FXS fibroblasts (see Fig. 1C) may be explained by high DNMT1 occupancy at the 5′UTR of the *FMR1* gene, which could reduce apparent enrichment in the IP, although other factors may also contribute. Additionally, as directly observed by EMSA and by DNMT1 activity ELISA assay, the binding avidity between the enzyme and the DNA:RNA hybrids stemming from the *FMR1* locus appeared more robust for hybrids formed between DNA template and mRNA than those formed between antisense transcript and no-template DNA strand, suggesting a regulatory function of DNMT1 in gene expression. To dynamically mimic the silenced or active status of *FMR1* gene (as in FXS or in control/PM/UFM cells, respectively), cells are pharmacologically treated with compounds able to inactivate or reactivate transcription. Despite transcriptional inhibition of *FMR1* active cells was not total, some features resemble those of inactive cells, such as FXS: reduction of hybrids at 5′UTR of *FMR1*

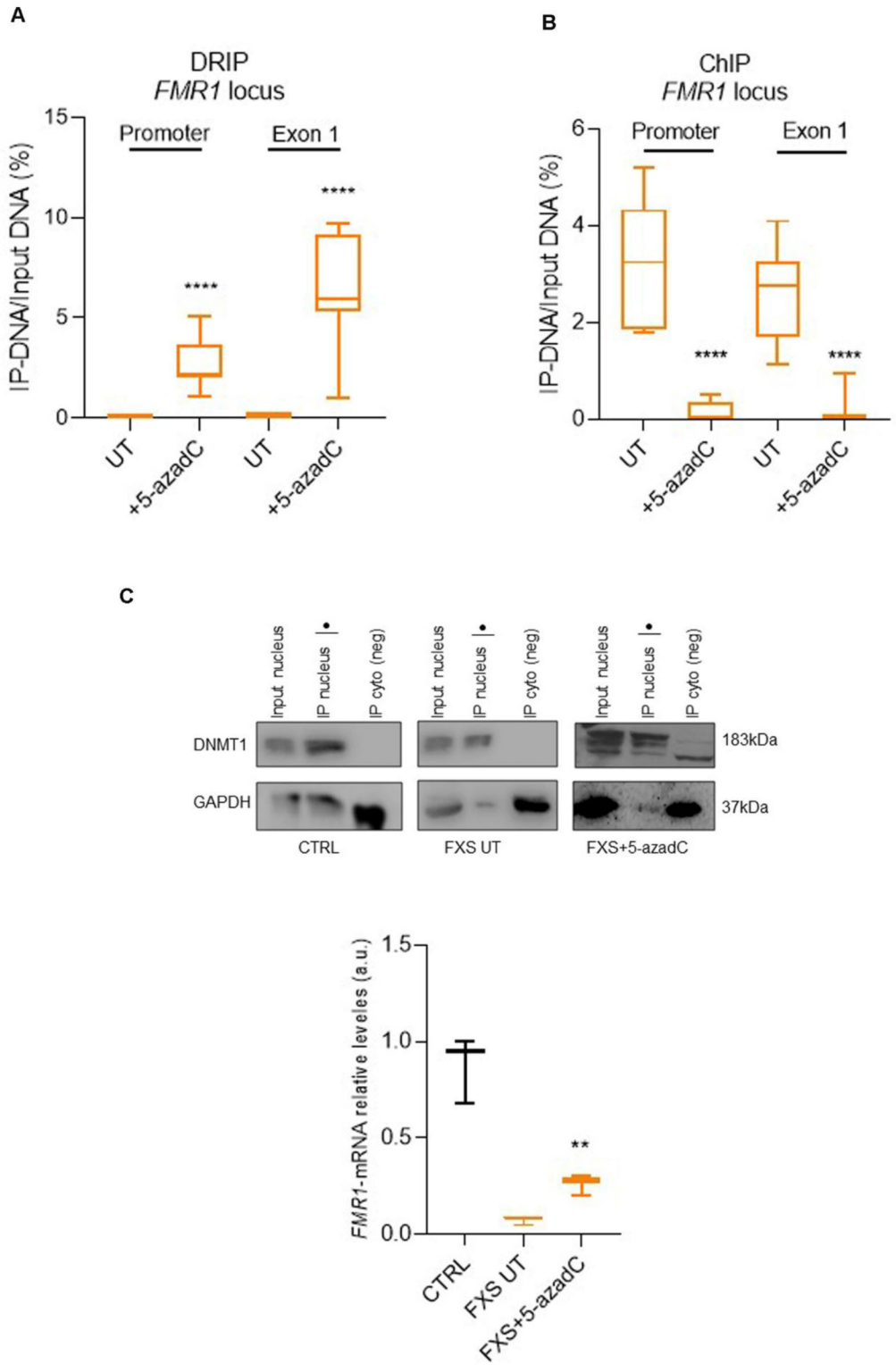

Figure 4. Transcriptional reactivation of the *FMR1* gene through 5-azadC treatment of FXS fibroblasts. (**A**) DRIP assay in FXS fibroblasts followed by absolute quantification of IP-DNA through qPCR using specific probe for *FMR1* promoter and exon 1 regions. After transcriptional reactivation with 5-azadC, levels of R-loops significantly increased in treated fibroblasts compared to the untreated cells. Three independent 5-azadC treatments are done ($n = 3$). (**B**) ChIP assay using antibody against DNMT1 in FXS fibroblasts treated with 5-azadC compared to untreated controls followed by absolute quantification of IP-DNA through qPCR using specific probes for *FMR1* promoter and exon 1 regions. After transcriptional reactivation through 5-azadC, levels of DNA bound to DNMT1 at the *FMR1* promoter and exon 1 regions are significantly decreased in treated cells compared to untreated controls. Three independent immunoprecipitations are done ($n = 3$); $^{****}P < 0.0001$ (Student's *t*-test versus untreated). (**C**) RIP using antibody against DNMT1 (on the top) followed by relative quantification by qPCR of *FMR1* transcript bound to DNMT1 in untreated and 5-azadC treated FXS compared to control (on the bottom). Note the enrichment of DNMT1 in the nuclear fraction after IP (black dot). After IP *FMR1*–mRNA bound to DNMT1 is quantified using qPCR comparing each sample to the corresponding input RNA. Relative levels of *FMR1*–mRNA bound to DNMT1 were slightly higher after 5-azadC treatment compared to untreated FXS. Three independent RIPs are performed (n = 3). $^{**}P < 0.01$ (Student's *t*-test versus untreated FXS).

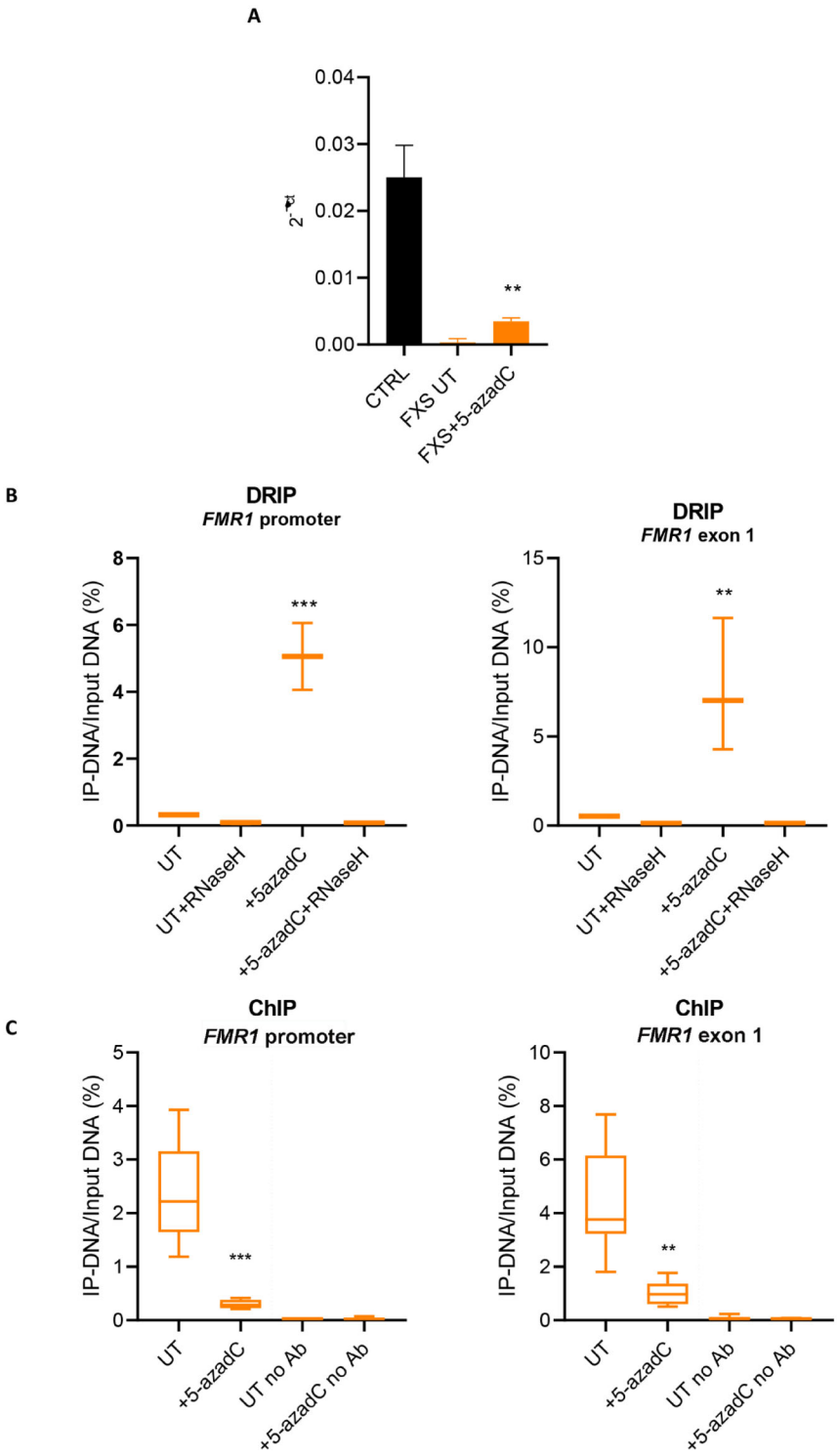

Figure 5. Transcriptional reactivation of the *FMR1* gene through 5-azadC treatment of FXS iPS-derived neurons. (**A**) Relative quantification of *FMR1*–mRNA after 5-azadC treatment of FXS iPS-derived neurons using qPCR. After 5-azadC treatment a significant increase of *FMR1* transcription is observed in silenced FXS iPS-derived neurons compared to the untreated control (UT), without reaching levels of *FMR1* transcription of control neurons. Three independent treatments with 5-azadC compound are performed ($n = 3$); $**P < 0.01$. (**B**) DRIP assay in FXS iPS-derived neurons followed by absolute quantification of IP-DNA through qPCR using specific probe for *FMR1* promoter (on the left) and exon 1 (on the right) regions after 5-azadC treatment. After transcriptional reactivation with 5-azadC, levels of R-loops significantly increased in treated neurons compared to the untreated cells. RNase H digested RNA in DNA:RNA hybrids ensuring the specificity of the signal. Three independent 5-azadC treatments are done ($n = 3$); $*P < 0.05$, $***P < 0.001$. (**C**) ChIP assay using antibody against DNMT1 in FXS iPS-derived neurons treated with 5-azadC compared to untreated controls followed by absolute quantification of IP-DNA through qPCR using specific probes for *FMR1* promoter (on the left) and exon 1 (on the right) regions. After transcriptional reactivation through 5-azadC, levels of DNA bound to DNMT1 at the *FMR1* promoter and exon 1 regions are significantly decreased in treated cells compared to untreated neurons. All samples are treated as the corresponding immunoprecipitated but without adding the antibody (no Ab), thus representing negative control. Three independent immunoprecipitations are done ($n = 3$); $**P < 0.01$, $***P < 0.001$ (Student's *t*-test versus untreated).

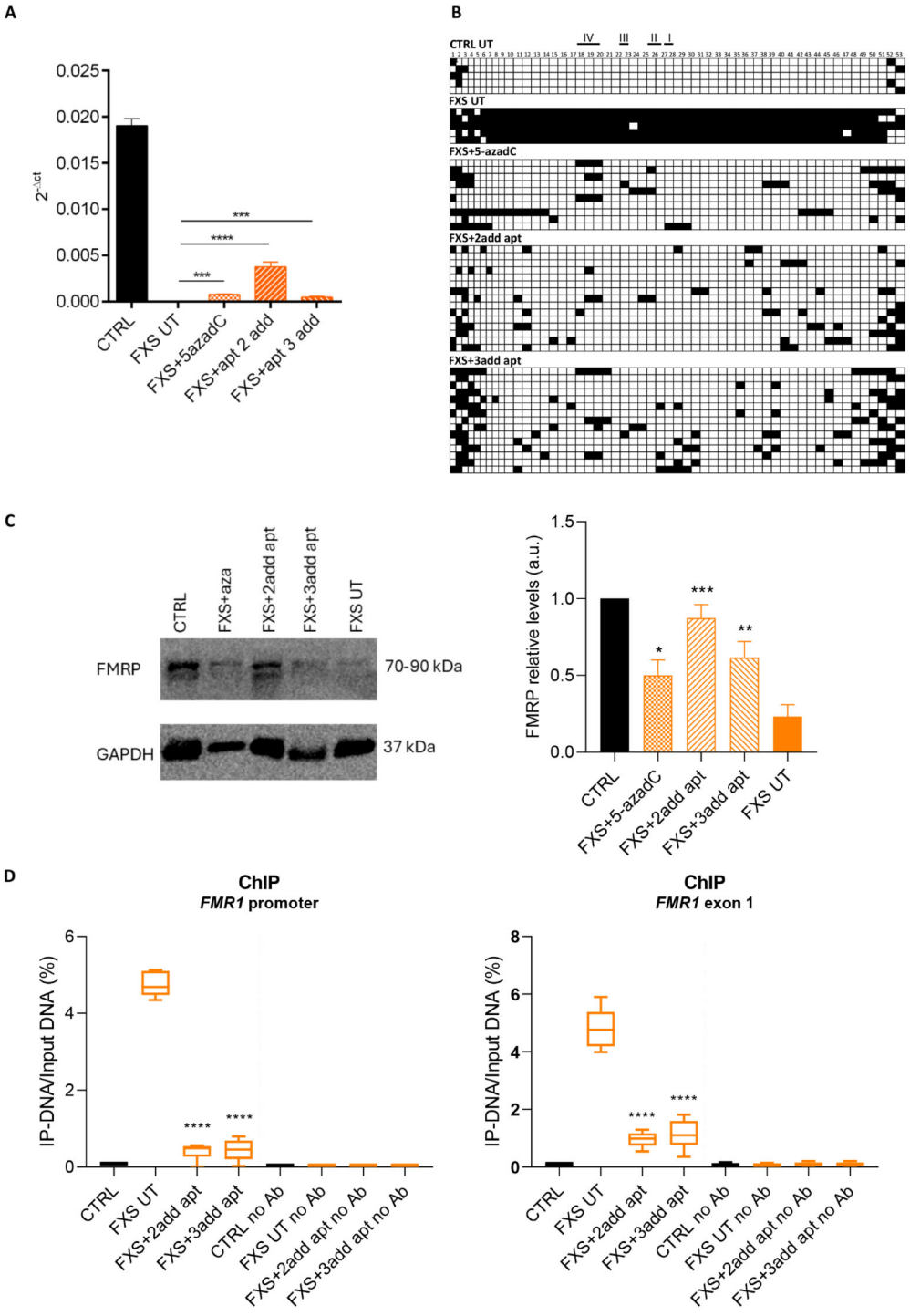

Figure 6. Transcriptional reactivation of the *FMR1* gene through DNMT1-specific aptamer on FXS iPS-derived neurons. (**A**) Relative quantification of *FMR1*–mRNA after aptamer transfection on FXS iPS-derived neurons using qPCR. After aptamer transfection a significant increase of *FMR1* transcription is observed in silenced FXS neurons compared to the untreated control (UT). FXS neurons are transfected with 2 and 3 doses of aptamer for three independent transfections ($n = 3$); $***P < 0.001$, $****P < 0.0001$ (Student's *t*-test versus untreated). (**B**) Bisulfite sequencing of the CGI of the *FMR1* promoter region after aptamer transfection of FXS iPS-derived neurons. White squares represented unmethylated cytosines, while black squares methylated positions. Binding sites for the main transcription factors are reported on the top (see also [31] and [32]). Note that after reactivation of *FMR1* transcription through aptamer transfection of FXS iPS-derived neurons, a reduction in DNA methylation is observed. (**C**) Representative WB of FXS iPS-derived neurons after aptamer transfection. FMRP levels reappeared after aptamer transfection in FXS neurons at an even higher level than that induced by 5-azadC. On the left, bars represented mean + SD of three independent protein lysates of three independent transfections ($n = 3$); $*P < 0.05$, $**P < 0.01$, $***P < 0.001$ (Student's *t*-test vs. untreated FXS). (**D**) ChIP assay using antibody against DNMT1 in FXS iPS-derived neurons transfected with aptamer compared to untreated controls followed by absolute quantification of IP-DNA through qPCR using specific probes for *FMR1* promoter (on the left) and exon 1 (on the right) regions. After transcriptional reactivation through aptamer, levels of DNA bound to DNMT1 at the *FMR1* promoter and exon 1 regions are significantly decreased in transfected cells compared to untransfected neurons. All samples are untransfected as the corresponding immunoprecipitated but without adding the antibody (no Ab), thus representing negative control. Three independent immunoprecipitations are done ($n = 3$); $****P < 0.0001$ (Student's *t*-test vs. untransfected).

locus, increased binding of DNMT1 to the *FMR1* gene and a surprising increased levels of DNA methylation at the *FMR1* promoter CGI. Treatment with DRB was able to augment methylation status of the *FMR1* promoter region in control, PM, and UFM cells, particularly at levels of footprints I, II, and IV that are binding sites for transcriptional factors such as Sp1, USF, and CREB [39, 40]. Increase in DNA methylation does not reach levels of that of FXS cells, in accordance with the fact that transcriptional inhibition of the *FMR1* was not fully complete. Complementarily, transcriptional reactivation of the *FMR1* gene with the demethylating agent 5-azadC on FXS cells does not normalize as in control cells, its levels of transcription remain at ∼30%–40% respect to normal control cells [22, 23, 31]. Given that transcription and translation of the *FMR1* locus increase and methylation of the CGI of the *FMR1* promoter region reduce [23, 31], treatment of FXS cells with 5-azadC restore hybrids at the *FMR1* locus and remove the methylation block represented by the DNMT1 binding to the locus. After the transcriptional reactivation induced by 5-azadC, part of the *FMR1* transcript is found to be bound to DNMT1. Similar results are obtained treating with 5-azadC neurons derived from FXS–iPSCs. Also, in differentiated cells, 5-azadC reduces DNMT1 bound to the *FMR1* locus allowing increase in *FMR1* transcription and consequently formation of R-loops at the 5'UTR of the locus.

Transcriptional reactivation of the *FMR1* gene in neurons derived from FXS-iPSCs after 5-azadC treatment does not reach normal levels, despite leads to restore a partial FMRP translation, as previously observed treating different cells [23]. Although 5-azadC is the only compound that robustly reactivates *FMR1* gene *in vitro*, its toxic side effects limit its clinical use in FXS patients [41, 42]; moreover it requires cell division to be incorporated, resulting difficult for the Fragile X target cells, i.e. neurons. Nevertheless, Bar-Nur *et al.* [43] treated FXS–iPS and their derived neurons with 5-azacytidine (5-azaC, a cytosine analogue similar to 5-azadC) and they observed a robust *FMR1* reactivation after treatment. Treatments with 5-azaC (and 5-azadC) were performed by other groups in differentiated neurons [44, 45] and in human FXS–neural cells transplanted in rodent brains, supporting the feasibility of gene reactivation in the context of CNS [46].These data represent surprising finding if considered that neurons are not dividing cells and expressed MAP2, a marker of differentiated neurons. In support of such results several papers demonstrated modulation in the expression of *BRCA1*, *reelin*, *BDNF*, and other genes in post-mitotic neurons using 5-azadC [47–49].

In an elegant work, using dCas9–Tet1/sgRNA approach, the authors restored the expression of *FMR1* in FXS iPSCs, demethylating the CGG expansion: the heterochromatin status of the *FMR1* promoter switched on to an active chromatin status [50]. Again, neurons derived from these edited FXS iPSCs rescued the electrophysiological abnormalities and restored a WT phenotype. Low amount of FMRP appeared sufficient for normalizing neuronal function [50, 51]. The overall impact of 5-azadC treatment was to assess its impact on the DNMT1-mediated regulation of *FMR1*. The results showed that 5-azadC treatment led to a robust reactivation of *FMR1* expression, further supporting the idea that DNMT1-mediated methylation of the *FMR1* locus is a key regulator of its transcription.

The main therapeutic goal is to specifically switch on the epigenetic block of the expanded *FMR1* gene in FXS, restoring gene expression and FMRP translation and reversing the neuronal anomalies due to the lack of FMRP. The exact sequence that leads to inactivation of the gene is not yet fully understood [52]. In human embryonic stem cells (hESCs) derived from FXS, that mimic the early stage of FXS embryo in which the *FMR1* locus is active until 11th week when it becomes silenced [53, 54], transcription of the expanded gene is maintained. During differentiation of FXS hESCs the epigenetic silencing leads to *FMR1* gene inactivation, thus resulting in a loss of FMRP. Using a small molecule, named 1a, able to disrupt the interaction of the mRNA with the expanded CGG portion of the *FMR1* gene prevented gene silencing [14]. This paper demonstrated that RNA is required for epigenetic silencing of the gene, but it is not fully described the exact mechanism underlying the inactivation mechanisms and does not explain the existence of UFM. A different small molecule known as 2HE–5Nme is able to specifically binds the CGG repeat expansion of the *FMR1* mRNA and prevents the resilencing of the gene after 5-azadC withdrawal also in FXS differentiated neurons [45]. Our preliminary transfection of FXS fibroblasts with an aptamer able to bind and inhibit DNMT1, restoring *FMR1*, represents a proof of concept of a molecular mechanism in which DNMT1 is a crucial enzyme in the epigenetic silencing of the *FMR1* gene [25]. The same aptamer was transfected in FXS differentiated neurons demonstrating its efficacy in *FMR1* transcriptional reactivation with partial rescue of FMRP translation particularly after two additions of the aptamer. A higher level of reactivation might be expected after three aptamer administrations; however, repeated transfections likely introduce cytotoxic effects. Future work should explore more efficient and less toxic delivery strategies for the aptamer. The use of aptamers targeting DNMT1 provides a promising approach to modulate the gene expression by interfering with the RNA interaction with DNMT1. The interplay between DNMT1, the *FMR1* locus, and its RNA highlights the intricate regulatory mechanisms governing gene expression. The ability to modulate this interaction using aptamers and methylation inhibitors, like already done with 5-azadC, could pave the way for new therapeutic strategies in treating FXS, offering hope for targeted interventions that restore normal gene expression and mitigate the effects of genetic disorders like FXS.

These findings suggest a potential targeted-therapeutic avenue for FXS. Further experiments will be focused on minimizing any off-target effects and optimizing the selectivity properties for CNS needed for a therapeutic intervention in FXS.

Limitations of the study: while our study provides new insights into the molecular reactivation of *FMR1* by aptamer treatment in FXS cells, several limitations should be acknowledged. First, the functional consequences of *FMR1* reactivation on neuronal activity and other cellular phenotypes were not addressed and will require dedicated future studies. Second, experiments were performed *in vitro* using iPSC-derived neurons and fibroblasts, which may not fully recapitulate the complexity of the human brain. Finally, although our analyses focused on selected molecular and epigenetic readouts, additional layers of regulation and long-term effects of *FMR1* reactivation remain to be explored. Addressing these points will be important in future work to fully

assess the therapeutic potential of aptamer-mediated *FMR1* reactivation.

Acknowledgements

We greatly acknowledge the Italian Association of Families with Fragile X syndrome to the continuous support to our research. We thank Aptadir Therapeutics for supporting the study.

Author contributions: Veronica Nobile (Investigation [lead], Writing – original draft [lead]), Benedetta Niccolini (Investigation [supporting]), Cecilia Pucci (Investigation [supporting]), Roberta Pietrobono (Methodology [equal]), Clarissa Modafferi (Investigation [supporting]), Carla Lucia Esposito (Investigation [supporting]), Natalia Cappoli (Investigation [supporting]), Giada Bianchetti (Investigation [supporting]), Giuseppe Maulucci (Writing – review & editing [supporting]), Giuseppe Aceto (Investigation [supporting]), Marcello D'Ascenzo (Writing – review & editing [supporting]), Pietro Chiurazzi (Writing – review & editing [supporting]), Cinzia Dello Russo (Writing – review & editing [supporting]), Maurizio Genuardi (Writing – review & editing [supporting]), Giovanni Neri (Writing – review & editing [supporting]), Annalisa Di Ruscio (Writing – review & editing [supporting]), and Elisabetta TABOLACCI (Conceptualization [lead], Writing – review & editing [lead])

Supplementary data

Supplementary data is available at NAR Molecular Medicine online.

Conflicts of interest

Annalisa Di Ruscio is a co-founder and serves as a scientific consultant for Aptadir Therapeutics. Elisabetta Tabolacci serves as a scientific consultant for Aptadir Therapeutics.

Funding

Our research was funded by Ministero dell'Università e della Ricerca under PRIN 2017 – ID: 201789LFKB and PRIN2022 – ID: 2022XTSLAP (to E.T.), PRIN2022 – ID: 20228HRTJ2 (to P.C.); Fondazione Policlinico Universitario 'A. Gemelli' IRCCS "Ricerca Corrente 2023" and "Ricerca Corrente 2024" (to E.T. and P.C.); the HIRM Pilot Award 2021, partially the ACS RSG-23-1036643-01-DMC and the NIDDK R01DK136116 (to A.D.R.).

Data availability

The data underlying this article are available in the article and in its online supplementary material.

References

1. Smeets HJ, Smits AP, Verheij CE *et al.* Normal phenotype in two brothers with a full FMR1 mutation *Hum Mol Genet* 1995;4:2103–8. https://doi: 10.1093/hmg/4.11.2103
2. Tabolacci E, Moscato U, Zalfa F *et al.* Epigenetic analysis reveals a euchromatic configuration in the FMR1 unmethylated full mutations *Eur J Hum Genet* 2008;16:1487–98. https://doi.org/10.1038/ejhg.2008.130
3. Tabolacci E, Chiurazzi P. Epigenetics, fragile X syndrome and transcriptional therapy. *Am J Med Genet A* 2013;161A:2797–808. https://doi.org/10.1002/ajmg.a.36264
4. Primerano B, Tassone F, Hagerman RJ *et al.*, Reduced FMR1 mRNA translation efficiency in fragile X patients with premutations *RNA* 2002;8:1482–8. https://doi.org/10.1017/S1355838202020642
5. Todd PK, Oh SY, Krans A *et al.* CGG repeat-associated translation mediates neurodegeneration in fragile X tremor ataxia syndrome *Neuron* 2013;78:440–55. https://doi.org/10.1016/j.neuron.2013.03.026
6. Loomis EW, Sanz LA, Chédin F *et al.* Transcription-associated R-loop formation across the human FMR1 CGG-repeat region *PLoS Genet* 2014;10:e1004294. https://doi.org/10.1371/journal.pgen.1004294
7. Thomas M, White RL, Davis RW. Hybridization of RNA to double-stranded DNA: formation of R-loops. *Proc Natl Acad Sci USA* 1976;73:2294–8. https://doi.org/10.1073/pnas.73.7.2294
8. Wahba L, Costantino L, Tan FJ *et al.* S1-DRIP-seq identifies high expression and polyA tracts as major contributors to R-loop formation *Genes Dev* 2016;30:1327–38. https://doi.org/10.1101/gad.280834.116
9. Ginno PA, Lott PL, Christensen HC *et al.* R-loop formation is a distinctive characteristic of unmethylated human CpG island promoters *Mol Cell* 2012;45:814–25. https://doi.org/10.1016/j.molcel.2012.01.017
10. Chen L, Chen JY, Zhang X *et al.*, R-ChIP using inactive RNase H reveals dynamic coupling of R-loops with transcriptional pausing at gene promoters. *Mol Cell* 2017;68:745–57. https://doi.org/10.1016/j.molcel.2017.10.008
11. Grunseich C, Wang IX, Watts JA *et al.* Senataxin mutation reveals how R-loops promote transcription by blocking DNA methylation at gene promoters *Mol Cell* 2018;69:426–37. https://doi.org/10.1016/j.molcel.2017.12.030
12. Ginno PA, Lim YW, Lott PL *et al.* GC skew at the 5' and 3' ends of human genes links R-loop formation to epigenetic regulation and transcription termination. *Genome Res* 2013;23:1590–600. https://doi.org/10.1101/gr.158436.113
13. Groh M, Lufino MMP, Wade-Martins R *et al.* R-loops associated with triplet repeat expansions promote gene silencing in Friedreich ataxia and fragile X syndrome. *PLoS Genet* 2014;10:e1004318. https://doi.org/10.1371/journal.pgen.1004318
14. Colak D, Zaninovic N, Cohen MS *et al.* Promoter-bound trinucleotide repeat mRNA drives epigenetic silencing in fragile X syndrome *Science* 2014;343:1002–5. https://doi.org/10.1126/science.1245831
15. Costantino L, Koshland D. The Yin and Yang of R-loop biology. *Curr Opin Cell Biol* 2015;34:39–45. https://doi.org/10.1016/j.ceb.2015.04.008
16. Niehrs C, Luke B. Regulatory R-loops as facilitators of gene expression and genome stability. *Nat Rev Mol Cell Biol* 2020;21:167–78. https://doi.org/10.1038/s41580-019-0206-3
17. Castellano-Pozo M, Santos-Pereira JM, Rondón AG *et al.* R loops are linked to histone H3 S10 phosphorylation and chromatin condensation *Mol Cell* 2013;52:583–90. https://doi.org/10.1016/j.molcel.2013.10.006
18. Wang J, Haeusler AR, Simko EA. Emerging role of RNA•DNA hybrids in C9orf72-linked neurodegeneration. *Cell Cycle* 2015;14:526–32. https://doi.org/10.1080/15384101.2014.995490
19. Bennett CL, Dastidar S, Arnold FJ *et al.* Senataxin helicase, the causal gene defect in ALS4, is a significant modifier of C9orf72 ALS G4C2 and arginine-containing dipeptide repeat toxicity. *Acta Neuropathol Commun* 2023;11:164. https://doi.org/10.1186/s40478-023-01665-z
20. Di Ruscio A, Ebralidze AK, Benoukraf T *et al.* DNMT1-interacting RNAs block gene-specific DNA methylation *Nature* 2013;503:371–6. https://doi.org/10.1038/nature12598
21. Vershkov D, Yilmaz A, Yanuka O *et al.* Genome-wide screening for genes involved in the epigenetic basis of fragile X syndrome

Stem Cell Rep 2022;17:1048–58. https://doi.org/10.1016/j.stemcr.2022.03.011
22. Chiurazzi P, Pomponi MG, Willemsen R *et al.* In vitro reactivation of the FMR1 gene involved in fragile X syndrome *Hum Mol Genet* 1998;7:109–13. https://doi.org/10.1093/hmg/7.1.109
23. Tabolacci E, Mancano G, Lanni S *et al.* Genome-wide methylation analysis demonstrates that 5-aza-2-deoxycytidine treatment does not cause random DNA demethylation in fragile X syndrome cells. *Epigenetics Chromatin* 2016;9:12. https://doi.org/10.1186/s13072-016-0060-x
24. Kumari D, Usdin K. Polycomb group complexes are recruited to reactivated FMR1 alleles in Fragile X syndrome in response to FMR1 transcription. *Hum Mol Genet* 2014;23:6575–83. https://doi.org/10.1093/hmg/ddu378
25. Esposito CL, Autiero I, Sandomenico A *et al.* Targeted systematic evolution of an RNA platform neutralizing DNMT1 function and controlling DNA methylation *Nat Commun* 2023;14:99. https://doi.org/10.1038/s41467-022-35222-4
26. Catuogno S, Esposito CL. Aptamer cell-based selection: overview and advances. *Biomedicines* 2017;5:49. https://doi.org/10.3390/biomedicines5030049
27. Brykczynska U, Pecho-Vrieseling E, Thiemeyer A *et al.* CGG repeat-induced FMR1 silencing depends on the expansion size in human iPSCs and neurons carrying unmethylated full mutations. *Stem Cell Rep* 2016;7:1059–71. https://doi.org/10.1016/j.stemcr.2016.10.004
28. Cerritelli SM, Crouch RJ. Ribonuclease H: the enzymes in eukaryotes. *FEBS J* 2009;276:1494–505. https://doi.org/10.1111/j.1742-4658.2009.06908.x
29. Drolet M, Phoenix P, Menzel R *et al.* Overexpression of RNase H partially complements the growth defect of an Escherichia coli delta topA mutant: R-loop formation is a major problem in the absence of DNA topoisomerase I. *Proc Natl Acad Sci USA* 1995;92:3526–30. https://doi.org/10.1073/pnas.92.8.3526
30. Haruki M, Noguchi E, Kanaya S *et al.* Kinetic and stoichiometric analysis for the binding of Escherichia coli ribonuclease HI to RNA-DNA hybrids using surface plasmon resonance. *J Biol Chem* 1997;272:22015–22. https://doi.org/10.1074/jbc.272.35.22015
31. Pietrobono R, Pomponi MG, Tabolacci E *et al.* Quantitative analysis of DNA demethylation and transcriptional reactivation of the FMR1 gene in fragile X cells treated with 5-azadeoxycytidine. *Nucleic Acids Res* 2002;30:3278–85. https://doi.org/10.1093/nar/gkf434
32. Lanni S, Goracci M, Borrelli L *et al.* Role of CTCF protein in regulating FMR1 locus transcription *PLoS Genet* 2013;9:e1003601. https://doi.org/10.1371/journal.pgen.1003601
33. Aceto G, Nardella L, Nanni S *et al.*, Glycine-induced activation of GPR158 increases the intrinsic excitability of medium spiny neurons in the nucleus accumbens. *Cell Mol Life Sci* 2024;81:268. https://doi.org/10.1007/s00018-024-05260-w
34. Aceto G, Nardella L, Lazzarino G *et al.* Acute restraint stress impairs histamine type 2 receptor ability to increase the excitability of medium spiny neurons in the nucleus accumbens. *Neurobiol Dis* 2022;175:105932. https://doi.org/10.1016/j.nbd.2022.105932
35. Boguslawski SJ, Smith DE, Michalak MA *et al.* Characterization of monoclonal antibody to DNA.RNA and its application to immunodetection of hybrids *J Immunol Methods* 1986;89:123–30. https://doi.org/10.1016/0022-1759(86)90040-2
36. Chodosh LA, Fire A, Samuels M *et al.* 5,6-Dichloro-1-beta-D-ribofuranosylbenzimidazole inhibits transcription elongation by RNA polymerase II *in vitro J Biol Chem* 1989;264:2250–7. https://doi.org/10.1016/S0021-9258(18)94169-4
37. Merry CR, Forrest ME, Sabers JN *et al.* DNMT1-associated long non-coding RNAs regulate global gene expression and DNA methylation in colon cancer *Hum Mol Genet* 2015;24:6240–53. https://doi.org/10.1093/hmg/ddv343
38. Zhao Y, Sun H, Wang H Long noncoding RNAs in DNA methylation: new players stepping into the old game. *Cell Biosci* 2016;6:45. https://doi.org/10.1186/s13578-016-0109-3
39. Chartier FL, Keer JT, Sutcliffe MJ *et al.* Construction of a mouse yeast artificial chromosome library in a recombination-deficient strain of yeast *Nat Genet* 1992;1:132–6. https://doi.org/10.1038/ng0592-132
40. Kumari D, Usdin K. The distribution of repressive histone modifications on silenced FMR1 alleles provides clues to the mechanism of gene silencing in fragile X syndrome. *Hum Mol Genet* 2010;19:4634–42. https://doi.org/10.1093/hmg/ddq394
41. Kaufmann M, Schuffenhauer A, Fruh I *et al.* High-throughput screening using iPSC-derived neuronal progenitors to identify compounds counteracting epigenetic gene silencing in fragile X syndrome. *J Biomol Screen* 2015;20:1101–11. https://doi.org/10.1177/1087057115588287
42. Kumari D, Swaroop M, Southall N *et al.* High-throughput screening to identify compounds that increase fragile x mental retardation protein expression in neural stem cells differentiated from fragile x syndrome patient-derived induced pluripotent stem cells. *Stem Cells Transl Med* 2015;4:800–8. https://doi.org/10.5966/sctm.2014-0278
43. Bar-Nur O, Caspi I, Benvenisty N. Molecular analysis of FMR1 reactivation in fragile-X induced pluripotent stem cells and their neuronal derivatives. *J Mol Cell Biol* 2012;4:180–3. https://doi.org/10.1093/jmcb/mjs007
44. Kumari D, Gazy I, Usdin K. Pharmacological Reactivation of the Silenced FMR1Gene as a Targeted Therapeutic Approach forFragile X Syndrome. *Brain Sci* 2019;9:1–18.
45. Kam CW, Dumelie JG, Ciceri G *et al.* Sustained epigenetic reactivation in fragile X neurons with an RNA-binding small molecule. *Genes (Basel)* 2025;16:278. https://doi.org/10.3390/genes16030278
46. Vershkov D, Fainstein N, Suissa S *et al.* FMR1 reactivating treatments in fragile X iPSC-derived neural progenitors *in vitro* and *in vivo*. *Cell Rep* 2019;26:2531–9. https://doi.org/10.1016/j.celrep.2019.02.026
47. Wang Q, Xu L, Chen P *et al.* Brca1 is upregulated by 5-Aza-CdR and promotes DNA repair and cell survival, and inhibits neurite outgrowth in rat retinal neurons. *Int J Mol Sci* 2018;19:1214. https://doi.org/10.3390/ijms19041214
48. Miller CA, Sweatt JD. Covalent modification of DNA regulates memory formation. *Neuron* 2007;53:857–69. https://doi.org/10.1016/j.neuron.2007.02.022
49. Pan Y, Daito T, Sasaki Y *et al.* Inhibition of DNA methyltransferases blocks mutant huntingtin-induced neurotoxicity *Sci Rep* 2016;6:31022. https://doi.org/10.1038/srep31022
50. Liu XS, Wu H, Krzisch M *et al.* Rescue of fragile X syndrome neurons by DNA methylation editing of the FMR1 gene *Cell* 2018;172:979–92. https://doi.org/10.1016/j.cell.2018.01.012
51. Graef JD, Wu H, Ng C *et al.* Partial FMRP expression is sufficient to normalize neuronal hyperactivity in Fragile X neurons *Eur J Neurosci* 2020;51:2143–57. https://doi.org/10.1111/ejn.14660
52. Nobile V Pucci C, Chiurazzi P *et al.*, DNA methylation, mechanisms of FMR1 inactivation and therapeutic perspectives for fragile X syndrome. *Biomolecules* 2021;11:296.
53. Eiges R, Urbach A, Malcov M *et al.* Developmental study of fragile X syndrome using human embryonic stem cells derived from preimplantation genetically diagnosed embryos. *Cell Stem Cell* 2007;1:568–77. https://doi.org/10.1016/j.stem.2007.09.001
54. Willemsen R, Bontekoe CJ, Severijnen L-A *et al.* Timing of the absence of FMR1 expression in full mutation chorionic villi. *Hum Genet* 2002;110:601–5. https://doi.org/10.1007/s00439-002-0723-5

Received: September 9, 2025. **Revised:** December 17, 2025. **Accepted:** January 2, 2026